Optical measures of dust velocities and direction during loss of vacuum accidents in confined environment and correlation between dust positions and properties with the resuspension degrees and the velocity modules

IOP Conf. Series: Journal of Physics: Conf. Series **882** (2017) 012011 doi:10.1088/1742-6596/882/1/012011

Optical measures of dust velocities and direction during loss of vacuum accidents in confined environment and correlation between dust positions and properties with the resuspension degrees and the velocity modules

Malizia Andrea[1,*] with Riccardo Rossi[2] and Pasquale Gaudio[2]

1. Department of Biomedicine and Prevention, University of Rome Tor Vergata, Via del Politecnico 1, 00133, Rome, Italy.
2. Department of Industrial Engineering, University of Rome Tor Vergata, Via del Politecnico 1, 00133, Rome, Italy.

*Corresponding author: malizia@ing.uniroma2.it

Abstract. Dust explosions are dangerous events that still today represent a risk to all the industries that produce and/or handle combustible dust like the agro-alimentary, pharmaceutical and energy ones. When a dust cloud is dispersed in an oxidant gas, like air, it may reach the explosive concentration range. A model to predict the dust critical conditions, that can cause explosions, is a key factor for safety of operators and the security of the plants. The key point to predict this dust resuspension is to measure the velocity vectors of dust under the accidental conditions. In order to achieve this goal the authors have developed an experimental facility, STARDUST-U, which allow to obtain different conditions of temperature and pressurization rates characteristic of accidents in confined environment. The authors have developed also optical methods and software to analyse different dust resuspension phenomena under different conditions in confined environment. In this paper, the author will present how they measure the dust velocity vectors in different experimental conditions (and for different type of dusts) and how they have related the dust characteristics and positions inside STARDUST-U with the resuspension degree and the velocity values.

1. Introduction

Despite the phenomenon of dust explosion has been known for more than 100 years, still today it is a dangerous hazard in process, medical, pharmaceutical, food, energetic, agribusiness industries and in any industrial plant that handles, produces and/or stores combustible dust [1, 2, 3]. Between the most recent and notable accidents there are the Imperial Sugar explosion [4], the Kunshan explosion and the Formosa Fun Coast explosion [3]. Table 1 shows the dust that led to dust explosion and the number of injuries and deaths [1, 4, 5].

Table 1. The most recent and notable accidents of dust explosions

Name of Event	***Source dust***	***Deaths***	***Injuries***
Imperial Sugar explosion (2008)	Sugar dust	14	42
Kunshan explosion (2014)	Metal powder	146	114
Formosa Fun Coast explosion (2015)	Coloured starch powder	15	498

It is well know that a dust explosion is a rapid combustion of dust finely dispersed in an oxidant gas. Several tests have been conducted to understand precisely the conditions that lead to dust explosions. These conditions are usually summarized through the dust explosion pentagon [2, 5-7]. The conditions that lead to dust explosions are:

1. ***Combustible dust***: Since combustion is an oxidation of the combustible, dust have to be oxidizable;
2. ***Oxidant***: The dust must be mixed inside an oxidant (usually air);
3. ***High concentration and fine dispersion:*** The rapid combustion is strongly correlated to the concentration level and how fine the dust is dispersed inside the oxidant [1, 8, 9];
4. ***Ignition source:*** It is needed to trigger the combustion [1];
5. ***Confinement:*** In some cases, confinement is not needed but usually strong improve the damages and the severity of the explosion [1].

Methods and techniques able to avoid that all these requests are reachable must be developed in order to make prevention of dust explosions. Prevention is the most important[10, 11].
The Quantum Electronics and Plasma Physics (QEP) research group develop and experimental apparatus called STARDUST-Upgrade [13]. It allows to replicate some thermos-fluid dynamic conditions that can provoke resuspension of dust in case of an under expanded-jet flowing inside a vacuum vessel that is typical of the accidents previously mentioned and also of accidents in energetic facilities [14,15].

The authors develop two optical experimental set-ups (similar to those of well known optical techniques like PIV and SHADOWGRAPH) to get images of mobilized dust under different thermos-fluid dynamic conditions. The first set-up that will be presented is used to acquire images when "bright" dust are used (like flour or stainless steel AISI316) and the second set-up is used to acquire images when "dark" dust are used (like carbon or tungsten).

In the first part of the paper results, we will present the images of experiments performed with flour that has been acquired, elaborated and analysed using software developed based on the Lucas-Kanade algorithm used to measure the dust velocity vectors. The velocity modules obtained will be compared with air velocity values (obtained experimentally in previous experimental campaign and numerically with FLUENT). In the second part of the paper results, we will elaborate data coming from experiments done using the 4 different types of dust, (to have 4 different density values) before mentioned changing, for each dust, the height from the bottom of the facility and changing the optical technique used to acquire images. It will be important to analyse three properties in function of the parameter δ and the density of dust: resuspension degree, mean velocity and max velocity. Intensity maps are discussed in order to understand when and how much the re-suspension can be dangerous.

2. Materials and Methods

STARDUST-Upgrade (Figure 1) is a stainless steel cylindrical tank. Thanks to its isolation from the external ambient, it can reach high vacuum values (till 100 Pa).

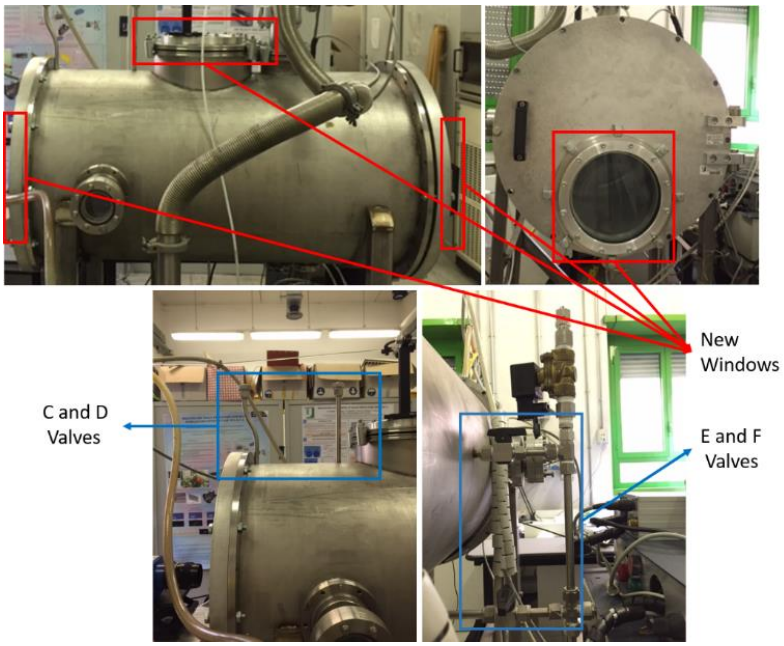

Figure 1. STARDUST-Upgrade: Windows and inlet valves.

Furthermore, a functional scheme of the facility is presented in Figure 2.

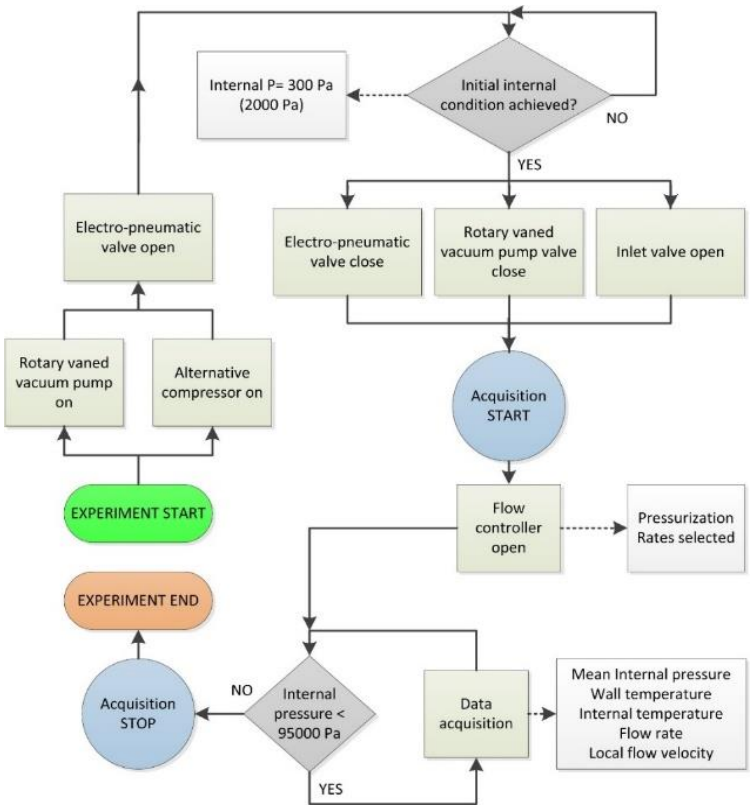

Figure 2. Experimental scheme of STARDUST-U

During each experiment, data acquisition was possible for the following quantities: thermocouples temperatures (T1 [°C], T2 [°C], T3 [°C], T4 [°C]), actual internal pressure (Ps [Pa]), inlet air flow rate

[litres/minutes]. Boundary conditions, in terms of initial internal pressure of the vacuum chamber (i.e. "vacuum level") and air flow rate entering the chamber, were achieved using a vacuum pump, and air compressed delivery system respectively, both remote controlled. The internal temperature was measured by four J-thermocouples placed inside the chamber. Internal pressure was measured by two gauges depending on the actual vacuum level. Edwards pressure gauge (ASG-2000-NW16, Edwards, Crawley, UK) covered pressure range from 1000 to 2000 mbar. For higher vacuum levels (pressure below 1000 mbar) a Pirani gauge was used (Alcatel AP 1004 Pirani Gauge, Alcatel Vacuum Technology). Pirani gauge covered a pressure range from 0.0005 to 1000 mbar. Air flow rate was controlled by a mass flow meter (1559A Mass-Flo® Controller, MKS Instruments) covering the range from 20 to 200 slm (standard litres per minute). Acquisition and control system was controlled remotely by a personal computer using a LabVIEW software. Acquisition hardware included an ethernet "CompactDAQ" chassis (NI cDAQ-9188XT) that allowed the introduction of 8 input/output cards.
Before the vacuum generation and loss of vacuum accident reproduction, a dust tray must be prepared and placed inside the camera. The tray has been covered by an opaque cardboard with the aim of decreasing the scattered light noise (Figure 3 a). Tray sizes are shown in Figure 3 b.

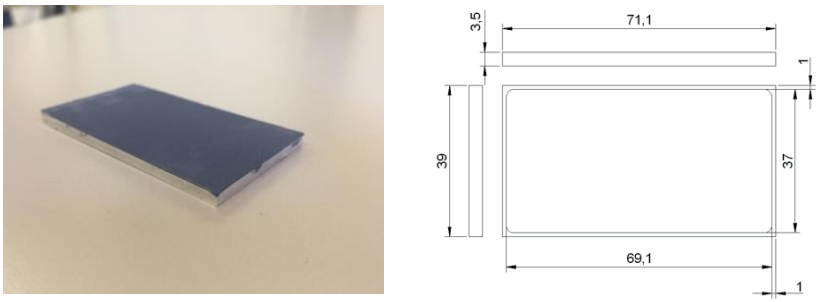

(a) *(b)*

Figure 3. Dust tray and opaque card board (a); Tray sizes (b).

The dust is deposited on the tray through a sieve, in order to decrease the larger agglomerate particles. In this work, dust samples are located on a tray placed in the center of the camera, along valve E and valve F with the possibility to change its height (Figure 4). An adimensional parameter δ calculated through (1) describes the relative distance between the inlet valve axis and the dust sample position.

$$Valve\ E:\ \ \delta = \frac{h_E - h_{Tray}}{d_{valve}} \quad (1)$$

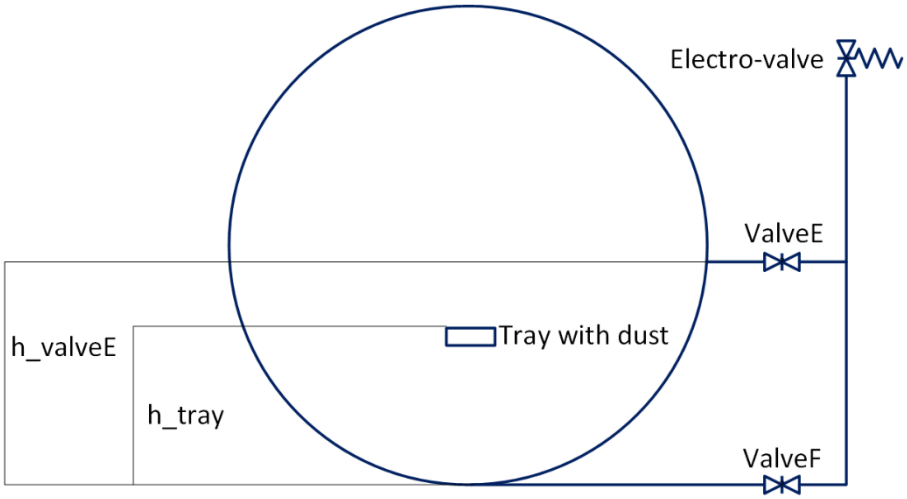

Figure 4. Valves and dust tray position and height parameters used.

STARDUST-Upgrade is provided with glass windows that allow the interface of devices to perform optical measurements. The aim of the work is to measure the velocity vectors of dust during an accident replication and then relate these measurements in function of the parameter δ and the density of dust mobilized. Four types of dust have been used: flour and stainless steel AISI316 (as bright powders), tungsten and carbon (graphite) powder (as dark powders). The particle velocities are measured through a method similar to Particle Tracking Velocimetry [19, 20, 21]. Anyway, since the characteristics of these dust are very different, two different optical setups have been used.
Table 2 describes the main characteristics of the light receiver and the light source of the two experimental setups.

Table 2. Main characteristics of optical experimental setups

Scattering setup		**Absorption setup**	
Light source	Diode Laser	*Light source*	Tungsten lamp
Wavelength	445 nm	*Wavelength*	White
Power	2 W	*Power*	Variable
Light receiver	CCD Fast Camera	*Light receiver*	CCD Fast Camera
Frame rate	5000 Hz	*Frame rate*	5000 Hz
Resolution	1280x128 pixels	*Resolution*	1280x128 pixels

The first experimental set-up (Figure 5) works well with "bright" dust, i.e. particles with a large scattering cross section (like flour of stainless steel in our case). A diode laser generates a laser sheet by means of two lenses, one convex and one cylindrical lens. The relative position of the two lenses allows to have larger or smaller laser sheet. The size of the laser sheet is fundamental to control the intensity of light that interacts with particles and so the intensity of the scattered light. The CCD fast camera is placed orthogonally to the laser sheet. Therefore, the fast camera record images with a dark background and white particles. The dust tracked with this setup is flour and stainless steel dust.

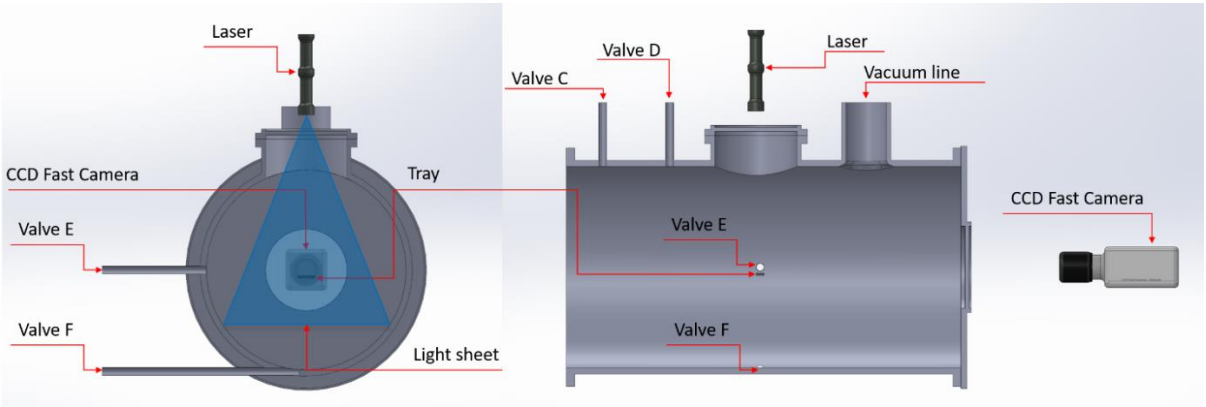

Figure 5. Optical setup to track particles with large scattering cross section.

Since "dark" particles have a too small scattering cross section (like tungsten and carbon in our case), another experimental setup (the second) is needed. In this case, a light source is placed on the same axis of the fast camera. Two convex lenses are used to parallelize the light source inside the camera (Figure 6).

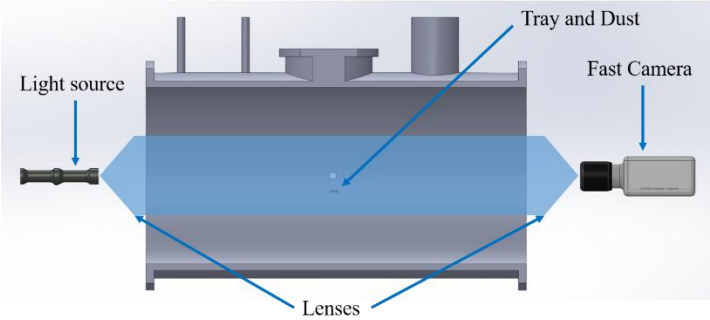

Figure 6. Optical setup to track particles with low scattering cross section and large absorption cross section.

Therefore, this technique record images with white background and black particles. This experimental setup must be used when the scattering cross section of dust particles is too low while absorption cross section is large enough. Anyway, since the software used to track particle works only if the particles are white, pre-processing of these images are needed. Figure 7 shows the main steps for pre-processing the images before velocity computation. Firstly, a background image is built. The background image is computed as the average of 100 frames where the dust is not moved and the inlet valve is not opened. The background image is inverted, therefore the black pixel becomes white and vice versa. Then, each i-image is inverted and the inverted background is subtracted to it. Therefore, the result is an image where only the particles in movement are white and the rest is black.

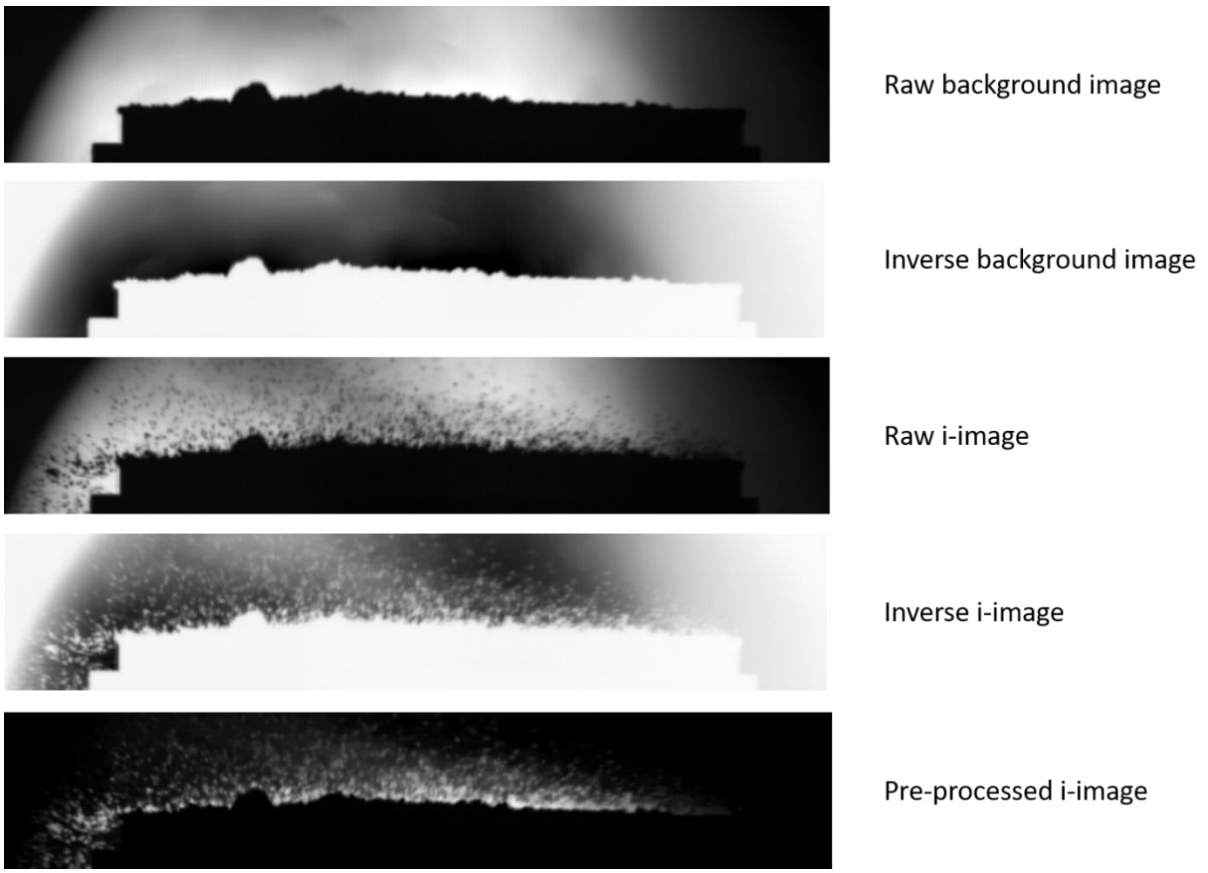

Figure 7. Pre-processing steps for large absorption cross section optical setup.

The software used [14] to track the velocity of the particles has been developed in LabVIEW language, with the aid of the National Instrument Vision tool. It detects the particles in the frame i-1 and looks for the same particles in the frame i. The algorithm used is the Lucas-Kanade algorithm [23, 24, 25].

In order to explain the Lucas Kanade Method we have to start from the basic concepts that a grayscale image is a matrix; The value of each matrix element is delimited between 0 (black) and 255 (White). All algorithms are based on brightness constancy. This hypothesis implies that an object cannot change its intensity along frames, but can vary its position (2).

$$I(x,y,t) = I(x+\delta x, y+\delta y, t+\delta t) \quad (2)$$

Where δx and δy are the pixel displacements and δt is the time difference between two frames. The aim of the optical software is to compute the displacements of each pixel.
Lucas&Kanade algorithm is one of the gradient-based methods. These are founded on developing brightness constancy hypothesis, which can be written as follows (3):

$$\frac{dI(x,y,t)}{dt} = 0 \quad (3)$$

And so, through partial derivations (4):

$$\frac{dI(x,y,t)}{dt} = \frac{\partial I}{\partial x}\frac{\partial x}{\partial t} + \frac{\partial I}{\partial y}\frac{\partial y}{\partial t} + \frac{\partial I}{\partial t} = 0 \;\rightarrow\; \frac{\partial I}{\partial x}u + \frac{\partial I}{\partial y}v + \frac{\partial I}{\partial t} = 0 \quad (4)$$

The idea of Lucas&Kanade algorithm consists in assuming a sub-matrix and doing the assumption that each pixel of that sub-matrix have the same velocity of the matrix itself. The algorithm performs (4) in each pixel of each block through (5) [26].

$$\begin{cases} \frac{\partial E}{\partial x}(p_1)\,u + \frac{\partial E}{\partial y}(p_1)\,v = -\frac{\partial E}{\partial t}(p_1) \\ \frac{\partial E}{\partial x}(p_2)\,u + \frac{\partial E}{\partial y}(p_2)\,v = -\frac{\partial E}{\partial t}(p_2) \\ \vdots \\ \frac{\partial E}{\partial x}(p_n)\,u + \frac{\partial E}{\partial y}(p_n)\,v = -\frac{\partial E}{\partial t}(p_n) \end{cases} \quad (5)$$

Furthermore, (5) can be written in matrix form (6):

$$C = \begin{bmatrix} \frac{\partial E}{\partial x}(p_1) & \frac{\partial E}{\partial y}(p_1) \\ \frac{\partial E}{\partial x}(p_2) & \frac{\partial E}{\partial y}(p_2) \\ \vdots & \vdots \\ \frac{\partial E}{\partial x}(p_n) & \frac{\partial E}{\partial y}(p_n) \end{bmatrix};\; \bar{v} = \begin{pmatrix} u \\ v \end{pmatrix}; d = \begin{bmatrix} -\frac{\partial E}{\partial t}(p_1) \\ -\frac{\partial E}{\partial t}(p_2) \\ \vdots \\ -\frac{\partial E}{\partial t}(p_n) \end{bmatrix} \quad (6)$$

$$C\bar{v} = d \rightarrow C^T C\bar{v} = C^T d \rightarrow \bar{v} = (C^T C)^{-1} C^T d \quad (7)$$

The final form, reached through (7), is (8).

$$\begin{pmatrix} u \\ v \end{pmatrix} = \begin{bmatrix} \sum \frac{\partial E}{\partial x}(p_i)^2 & \sum \frac{\partial E}{\partial x}(p_i)\frac{\partial E}{\partial y}(p_i) \\ \sum \frac{\partial E}{\partial x}(p_i)\frac{\partial E}{\partial y}(p_i) & \sum \frac{\partial E}{\partial y}(p_i)^2 \end{bmatrix}^{-1} * \begin{bmatrix} -\sum \frac{\partial E}{\partial x}(p_i)\frac{\partial E}{\partial t}(p_i) \\ -\sum \frac{\partial E}{\partial y}(p_i)\frac{\partial E}{\partial t}(p_i) \end{bmatrix} \quad (8)$$

In order to compute high velocities, LK algorithm needs a pyramidal implementation, which allows the algorithm to find high-velocity vectors. It is a very popular algorithm in optical method but sometimes heavy filtering function is required because of its high noise sensibility. LK algorithm implementation can be used also for feature point track. Pyramidal implementation consists in creating pyramid representation of each frame and computing point displacement in each representation. Through this expedient, maximum trackable velocity becomes $u_{max,p}=(2^{Lm+1}-1)u_{max}$ [27].

Pyramid images computation has been implemented to allow the computation of large velocity [28]. The output velocity of the algorithm is described in pixels/frame. Spatial conversion is computed measuring the pixel dimension in meters while the temporal conversion is obtained by the frame rate of the fast camera (5000 Hz).
The software has one graphic output that is the frame i with overlaid the particle velocity vectors (Figure 8) and a .txt file with all the velocity vectors information: x and y position, time, magnitude and angle.

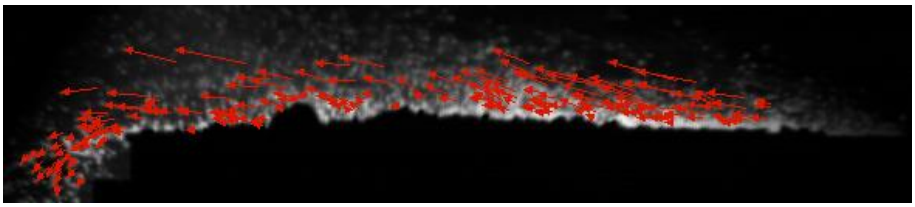

Figure 8. Frame i with the overlaid velocity vectors of the moving particles.

3. Results

In this first part we will analyze only the results coming from an experiment done with flour with the air inlet coming from Valve E and the dust tray placed at the same height of the dust. The software has been used to analyze the dust velocity vectors (modules and direction) and to compare the modules values to those of air flow jet (obtained experimentally and numerically [14-15]). In table 3, there are the experiments parameter:

Table 3. ValveE_0cm – Feature Table.

Valve	E
f_{acq} [Hz]	5000
Exposure time [s]	1/6000
Resolution [Pixel]	1280x128
Spatial res [m/px]	0,0001143
Z (cm to jet axis)	0
Number of Frame	3000
Initial dust weight [g]	2,9607
Final dust weight [g]	0
Dust mobilised [%]	100

Total mobilisation time [s]	0,496

Module and direction velocity correlation (Figure 9a) shows how highest velocities are parallel to jet main direction (0°) which is also the main particle direction (Figure 9b). Figure 10 shows the velocity histogram, showing the low number of high velocity particles compared to the low velocity particles.

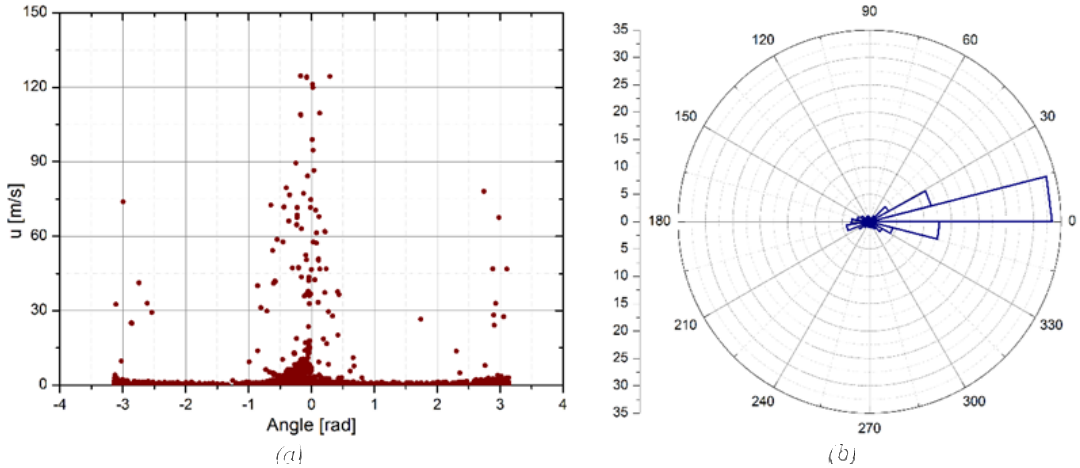

Figure 9. Module vs Direction Dust Particle Velocity (a) and Direction Polar Histogram (b).

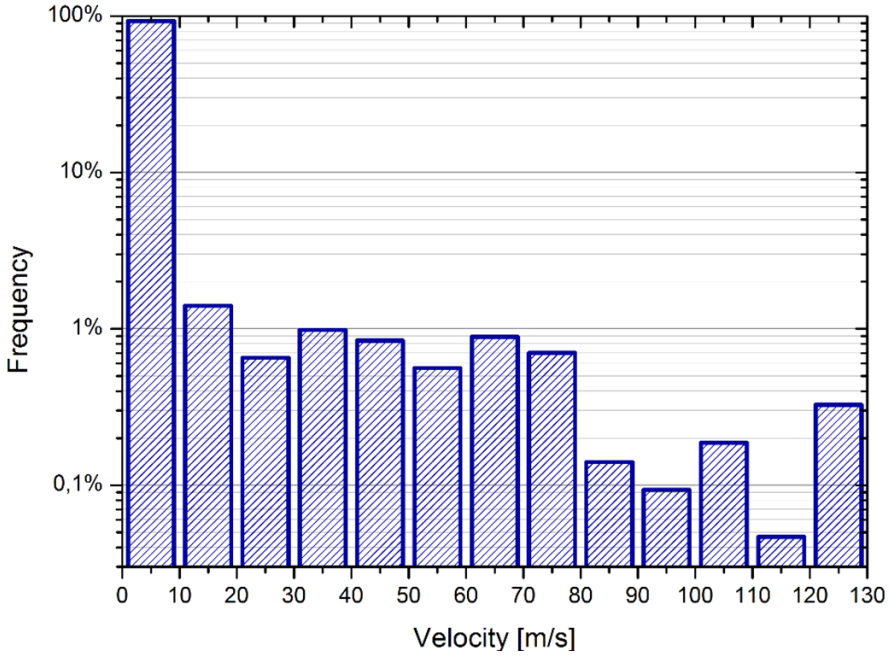

Figure 10. Velocity histogram

Figure 11 shows the correlation between tracked particles and experimental and numerical air jet. It illustrates only the first 0,6 s of the accidents, which is the time required to mobilise all the dust. Only few particles reach the experimental air jet velocity, while the majority does not reach 15 m/s. This occurs because slowest particles are the largest and consequently easier to be tracked. The largest particles are not single particles but agglomerates. The highest velocities are reached at the beginning of the experiment. It may be due to the fact that smaller particles mobilise immediately.

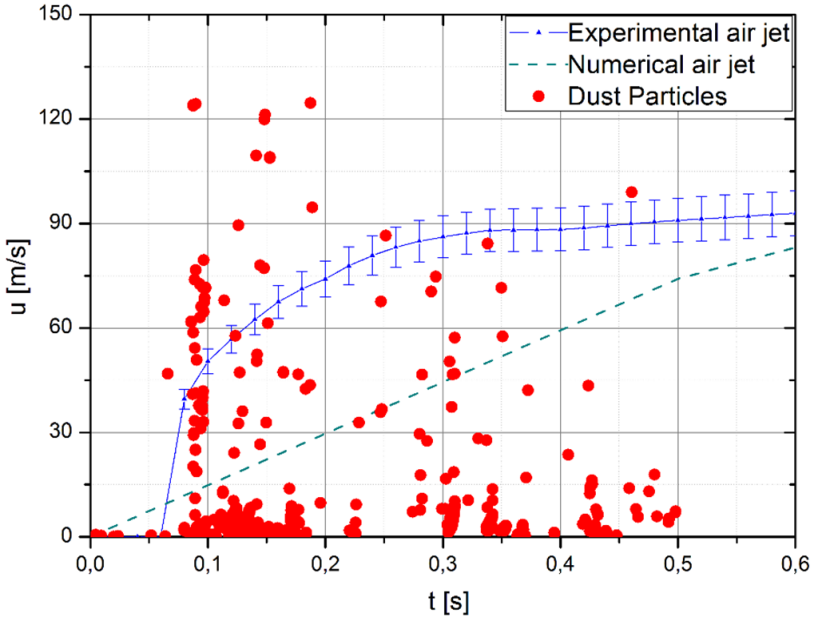

Figure 11. Dust particle velocities compared to experimental and numerical Air Jet velocity.

In Figure 12 there are the velocity vectors at different times.

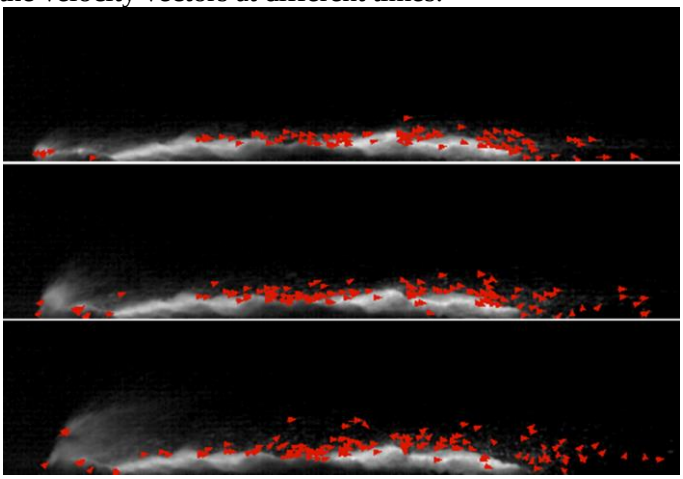

Figure 12. Velocity vectors at t_1=0,0886 s, t_2=0,0896 s and t_3=0,0910s

In the second phase we will elaborate data coming from experiments done using the 4 different types of dusts (to have 4 different density values) before mentioned changing, for each dust, the height from the bottom of the facility and changing the optical technique used to acquire images. It is important to analyse three properties in function of the parameter δ and the density of dusts: resuspension degree, mean velocity and max velocity.
Resuspension degree is calculated as (9):

$$\Delta m_{\%} = \frac{m_i - m_f}{m_i} \tag{9}$$

The mobilization of dust is characterised mainly by two forces: the aerodynamic resistance, drag, which moves particles, and the inter-particles and particle-wall friction forces, which slows down or

completely stop the dust mobilization. The drag aerodynamic resistance is a force that is dependent on air-particle relative velocity and fluid density, i.e. the dynamic pressure of the fluid (since the particles are not moving). Frictions forces are a function of dust and wall surface characteristics [29-31]

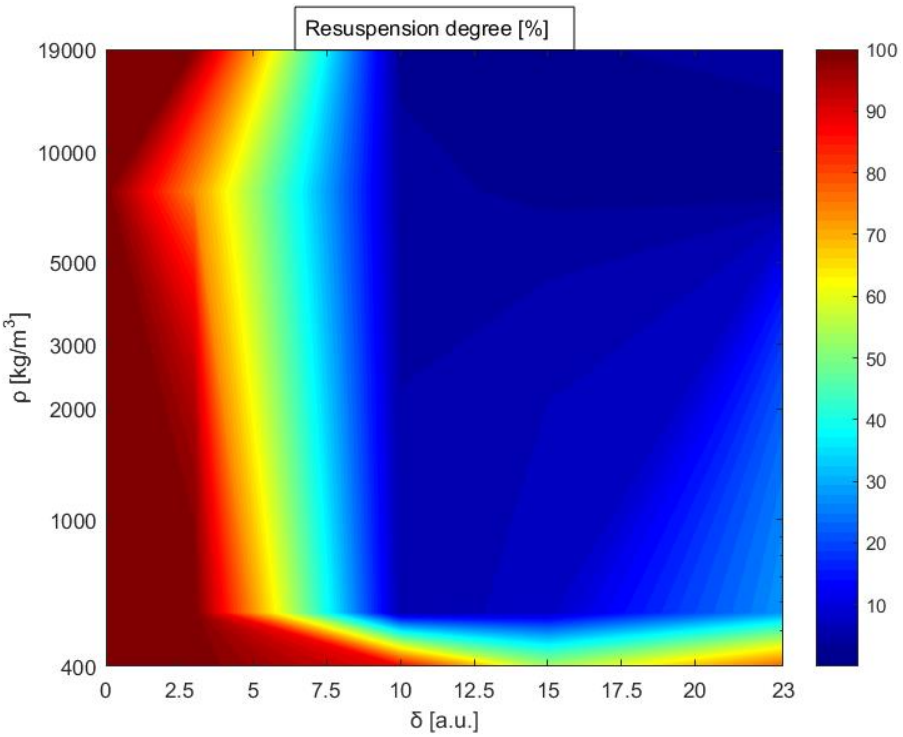

Figure 13. Resuspension degree map.

Figure 13 shows the re-suspension degree in function of density and δ parameter. When the tray with dust is placed at the same height of the valve (δ=0), the dust is completely mobilized, independently of its density. Increasing the distance of the tray from the inlet valve, the re-suspension degree falls down for any type of dust, excluded the lighter one (graphite dust). The minimum of re-suspension is reached for δ=15 while for higher values there is a slight increase. That increase is due to the specific flow inside STARDUST-U vessel. When the air flows inside from the valve E, two counter-vorteices are produced. The center of these vortices are the regions where the dynamic pressure is smaller. Therefore, since the vortex center height is around δ = 10 – 15, the re-suspension degree is minimized. Density of dust plays an important role, since for very small density the re-suspension is always very large, while with its decrease the re-suspension degree falls down.

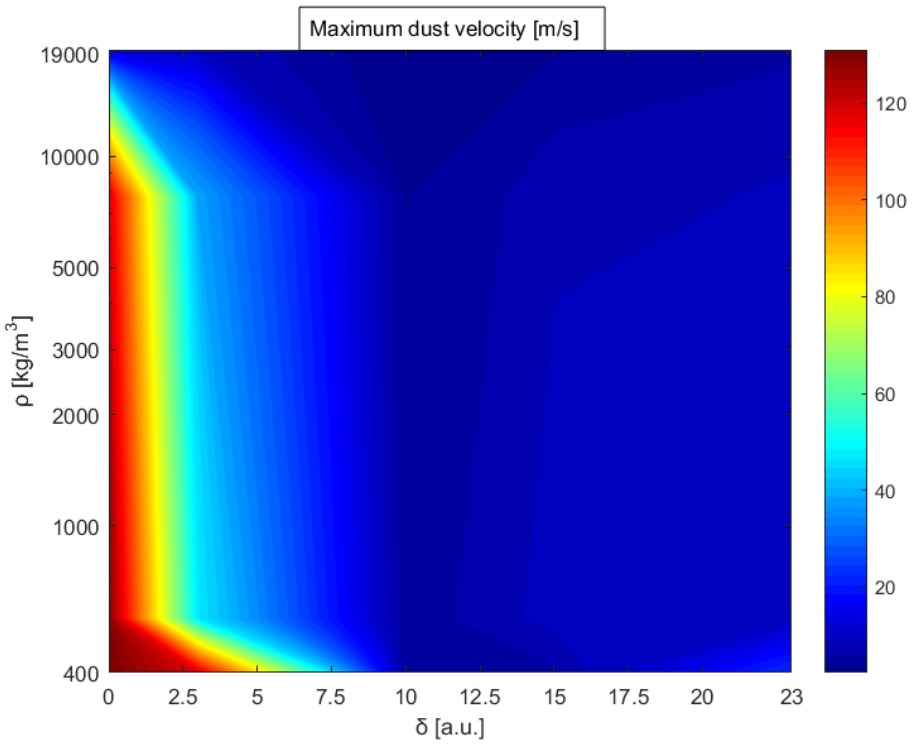

Figure 14. Maximum dust velocity map.

Figure 14 shows the maximum velocity reached by the particles. Still in this case we have a very large velocity only for δ = 0 and for lower density. The velocity map can be explained taking into account a simplified equation that describes the motion of a particle in a flow (9):

$$m_p \frac{du_p}{dt} = D = \frac{1}{2}\rho_f (u_f - u_p)^2 S_p c_d \qquad (9)$$

From the particle-motion equation is clear that the maximum velocity reachable by the dust particles is the local fluid velocity. Therefore, since the air velocity is very large only along the inlet valve axis, the dust maximum velocity follow the same trend. Moreover, the inertia of the particle is proportional to its mass and so its density. Then, the decrease of velocity in function of density is explained.

Equation (9) describes correctly the motion of a particle when the volume fraction of the disperse phase is very low. Therefore, it can be applied to explain the maximum velocity, since it is reached only by that particles detached from the re-suspension region, where the volume fraction are near to the maximum packing of the dust and so, with large friction due to particle-particle interactions.

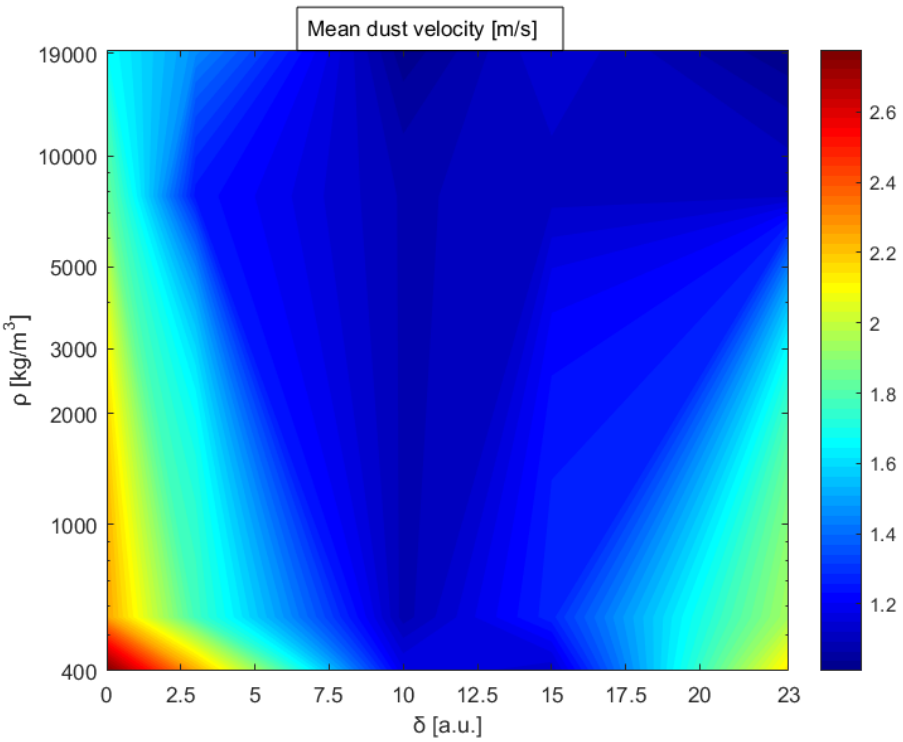

Figure 15. Mean dust velocity map.

Figure 15 shows the mean velocity trend. Still again, the maximum value is reached only for very low density and relative distance equal to zero. The minimum values are placed in the center of the vortex ($\delta \approx 10$) and with the large density of dust (tungsten). Dust density seems to play a larger role in mean velocity, since for each δ, as the density increase the mean velocity decrease.

The resuspension maps demonstrate that strong and dangerous re-suspension occur only if the film of dust is placed very closed to the isolation rupture or where the dynamic pressure of the flow is very large. Furthermore, the study of the continuum phase, in particular of the dynamic pressure field, could be sufficient to understand qualitatively where and how much dust can re-suspend.

The optical measurement techniques could be improved in order to develop a monitoring apparatus to control the concentration and velocity of dust in industrial plants.

4. Conclusion

The authors showed the measurements of dust re-suspension in case of loss of vacuum accident replicated in experimental apparatus called STARDUST-Upgrade. Non-invasive diagnostics involving imaging techniques have been implemented by the authors to perform dust tracking experiments that produced data on dust velocity vectors comparable to the figures for air velocity, that was measured with pressure transducers. Re-suspension degree has been measured through a precision balance. Optical measurements allowed to measure the mean and maximum velocity of mobilized particles. Since dust particles have different optical properties, two experimental setups have been developed. The first one is based on the scattering cross section of the dust while the second one with particles that has large absorption cross section. The experiments have been conducted changing the relative distance between the dust tray and the inlet valve. Then, re-suspension, maximum and mean velocity map have been built in order to study the influence of the parameter δ and the density of dust. Both the two parameters show an influence on the three dispersed phase characteristics. A minimum value of the re-suspension degree and velocity is reached when the dust tray is placed in the center of one of

the two counter rotating vortexes, which is characterised with the minimum of the dynamic pressure of the continuum phase. The results demonstrate how the re-suspension problem could be faced, qualitatively, studying the characteristics of the continuum phase. Anyway, if we are interested in accurately results, the best way is the use of multiphase computational fluid dynamic codes. In future, the QEP group will continue to collect experimental results in function of other characteristics, such as flow rate, temperature and initial pressure. Then, numerical simulation with identical boundary condition will be compared with the experimental data in order to validate it. Finally, an optical device able to measure dust characteristics could be developed to perform monitoring of re-suspension inside the industrial plants.

References

[1] R. K. Eckhoff, 2003, *Dust Explosions in the Process Industries*.
[2] Malizia A. et all, 2017, *A novel facility to investigate dust mobilization in confined environments with applications to the security of the pharmaceutical industry* , Materials Science Forum, ISSN: 1662-9760, Vol. 879, pp 1213-1219,
[3] Z. Yuan, N. Khakzad, F. Khan e P. Amyotte, 2015, *Dust explosion: A threat to the process industries,* Process Safety and Enviromental Protection, vol. 98, pp. 57-71
[4] U.S. Chemical Safety and Hazard Investigation Board, 2009, *Investigation Report: Sugar Dust Explosion and Fire*
[5] U.S.Chemical Safety and Hazard Investigation Board, 2005, *Investigation Digest - Dust Explosion at West Pharmaceutical Services*
[6] R. K. Eckhoff, 1996, *Prevention and Mitigation of dust explosions in the process industries: A survey of recent research and development*, J. Loss Prev. Process. Ind., vol. 9, n. 1, pp. 3-20,
[7] R. Eckhoff, 2005, *Current status and expected future trends in dust explosion research*, vol. 18, pp. 225-237.
[8] R. Eckhoff, 2009 *Understanding dust explosions. The role of powder science and technology*, J. Loss Prevent. Proc.
[9] J. Yuan, W. Wei, W. Huang, B. Du, L. Liu e J. Zhu, 2014, *Experimental investigations on the roles of moisture in coal dust explosion*, Journal of the Taiwan Institute of Chemical Engineers, vol. 45, n. 5, pp. 2325-2333,
[10] W. Gao, T. Mogi, J. Sun, J. Yu e R. Dobashi, 2013, *Effects of particle size distributions on flame propagation mechanism during octadecanol dust explosions*, Powder Technology, vol. 249, pp. 168-174.
[11] T. Abbasi e S. Abbasi, 2007, *Dust explosions-Cases, causes, consequences, and control,» Journal of Hazardous Materials*, vol. 140, n. 1-2, pp. 7-44.
[12] M. Abuwser, P. Amyotte, F. Khan e L. Morrison, 2013, *An optimal level of dust explosion risk management: Framework and application*, Journal of Loss Prevention in the Process Industries, vol. 26, n. 6, pp. 1530-1541.
[13] A. Malizia, M. Gelfusa, G. Francia, M. Boccitto, M. D. Vecchio, D. D. Giovanni, M. Richetta, C. Bellecci and P. Gaudio, 2014 , *Design of a new experimental facility to reproduce LOVA and LOCA consequences on dust resuspension*, Fusion Eng. Des.
[14] L. A. Poggi, A. Malizia, J. F. Ciparisse, M. Gelfusa, A. Murari, S. Pierdiluca, E. Lo Re, P. Gaudio. 2016. *First Experimental Campaign to Demonstrate STARDUST-Upgrade Facility Diagnostics Capability to Investigate LOVA Conditions*. J Fusion Energ, 34:1320-1330.
[15] J.F. Ciparisse, A. Malizia et all. 2015, *First 3D numerical simulations validated with experimental measurements during a LOVA reproduction inside the new facility STARDUST-Upgrade*. Fusion Engineering and Design 101, 204–208.
[16] C. Murillo, O. Dufand, N. Bardin-Monnier, O. Lopez, F. Munoz e L. Perrin, 2013. *Dust explosions: CFD modeling as a tool to characterize the relevant parameters of the dust dispersion*, Chemical Engineering Science, vol. 104, pp. 103-116.

[17] A. Malizia, L. A. Poggi, J.-F. Ciparisse, R. Rossi, C. Bellecci and P. Gaudio, 2016. *A Review of Dangerous Dust in Fusion Reactors: from Its Creation to Its Resuspension in Case of LOCA and LOVA*, Energies, vol. 9, no. 8,
[18] J. Ciparisse, A. Malizia, L. Poggi, M. Gelfusa, A. Murari, A. Mancini and P. Gaudio, 2015. *First 3D numerical simulations validated with experimental measurements during a LOVA reproduction inside the new facility STARDUST-Upgrade*, Fusion Eng. Des.,
[19] F. Scarano, 2002. *Iterative image deformation methods in PIV*, Meas. Sci. Technol., vol. 13, pp. R1-R19.
[20] C. Cierpka, N. A., Buchmann, J. Soria and C. J. Kahler, 2014. *Ultra-High-Speed 3D Astigmatic PTV in Supersonic Underexpanded Impinging Jets*, in 17th Int Symp on Applications of Laser Techniques to Fluid Mechanics, Lisbon, Portugal.
[21] L. Souverein, 2006. *PIV based aerodynamic loads determination in supersonic flows*, Delft,
[22] R. Rossi, A. Malizia, L. A. Poggi, E. Peluso e P. Gaudio, , 2016 . *Flow Motion and Dust Tracking Software for PIV and Dust PTV*, Journal of Failure Analysis and Prevention, vol. 2016, pp. 1-12.
[23] B. Schunck, K. P. Horn and B. G. 1980. *Determining Optical Flow*, Artif. Intell., pp. 185-203,
[24] B. D. Lucas and T. Kanade, 1981. *An Iterative Image Registration Technique with an Application to Stereo Vision*, Proceedings of Imaging Understanding Workshop, pp. 121-130.
[25] E. Meinhardt-Llopis, J. Sanchez and D. Kondermann, 2013. *Horn–Schunck Optical Flow with a Multi-Scale Strategy*, Image Processing On Line, pp. 151-172,
[26] B. D. Lucas and T. Kanade, 1981. *An Iterative Image Registration Technique with an Application to Stereo Vision*, Proceedings of Imaging Understanding Workshop, pp. 121-130.
[27] J. Bouguet, *Pyramidal Implementation of the AÆne Lucas Kanade Feature Tracker Description of the Algorithm*, Intel Corporation - Microprocessor Research Labs.
[28] J. Bouguet, *Pyramidal Implementation of the AÆne Lucas Kanade Feature Tracker Description of the Algorithm*, Intel Corporation - Microprocessor Research Labs.
[29] C. E. Brennen 2005, *Fundamentals of Multiphase Flows*, Pasadena, California: Cambridge University Press,
[30] F. Zhanf, M. Reeks e M. P. Kssane, 2012. *Particle Resuspension in Turbulent Boundary Layers and the Influence of Non-Gaussian Removal Forces*, Journal of Aerosol Science, vol. 58.
[31] O. G. Chkhetiani, E. B. Gledzer, M. S. Artamonova e M. A. Iordanskii, 2012. *Dust resuspension under weak wind conditions: direct observations and model*. Atmos. Chem. Phys., vol. 12, pp. 5147-5162.

Acknowledgements
As first author and principal investigator of this work, I want to thank Riccardo Rossi than help me in perform the experimental campaigns and Pasquale Gaudio that help me to mount the optical set-up.